

Non-Local Multi-Continuum method (NLMC) for Darcy-Forchheimer flow in fractured media

Denis Spiridonov ^{*} Maria Vasilyeva [†]

April 27, 2023

Abstract

This work presents the application of the non-local multicontinuum method (NLMC) for the Darcy-Forchheimer model in fractured media. The mathematical model describes a nonlinear flow in fractured porous media with a high inertial effect and flow speed. The space approximation is constructed on the sufficiently fine grid using a finite volume method (FVM) with an embedded fracture model (EFM) to approximate lower dimensional fractures. A non-local model reduction approach is presented based on localization and constraint energy minimization. The multiscale basis functions are constructed in oversampled local domains to consider the flow effects from neighboring local domains. Numerical results are presented for a two-dimensional formulation with two test cases of heterogeneity. The influence of model nonlinearity on the multiscale method accuracy is investigated. The numerical results show that the non-local multicontinuum method provides highly accurate results for Darcy-Forchheimer flow in fractured media.

Keywords: Darcy-Forchheimer model, non-local multicontinuum method, multiscale model reduction, finite volume method, embedded fracture model, fractured domain, nonlinear flow problem.

1 Introduction

Fluid flow in porous media is an essential element in understanding oil and gas production processes, as well as in reservoir hydrology, environmental protection, and many other [1–3]. Properly describing fluid properties and their movement in the reservoir is necessary for the model construction process to solve the problems of designing field development systems. This task requires accurately describing fluid and gas flow under actual reservoir conditions. Mathematical modeling is often used to select the best option for oil and gas field development. Modeling helps test various hydrocarbon production technologies, find the best options for production well placement schemes, and determine changes in physical oil and gas parameters [4–6].

^{*}Laboratory of Computational Technologies for Modeling Multiphysical and Multiscale Permafrost Processes, North-Eastern Federal University, 677000 Yakutsk, Republic of Sakha (Yakutia), Russia. Email: d.stalnov@mail.ru.

[†]Department of Mathematics and Statistics, Texas A&M University, Corpus Christi, Texas, USA. Email: maria.vasilyeva@tamucc.edu.

The fundamental law of fluid flow in porous media is Darcy’s law; it expresses the dependence of fluid filtration rate on the pressure gradient. Many scientific works are devoted to checking and investigating the limits of applicability of Darcy’s law [7–9]. In the case when the filtration rate is relatively high, inertial effects cannot be ignored, and the Darcy-Forchheimer model should be used [10–12]. Moreover, a high filtration rate can occur in highly heterogeneous and fractured media. In the fractures continuum, the flow velocity is much higher than in porous media [13]. In this paper, we consider the multiscale method for the nonlinear flow model in a fractured porous medium based on the Darcy-Forchheimer model [14].

Standard modeling approaches imply well-known approximation methods on a fine grid. The finite element or finite volume method is well-proven in mathematical modeling [15–17]. For modeling the Darcy-Forchheimer model, the mixed finite element method is commonly used to preserve the mass conservation on the discrete level [18–20]. This paper uses the finite volume method to solve a problem on the fine grid [21–24]. For the problem in fractured media, we should carefully choose the method for the approximation. The most straightforward way to approximate fractures based on the explicit fracture representation on the grid with the application of the discrete fracture model (DFM) for their approximation [25–27]. However, the DFM approach requires the construction of a very detailed grid with a vast number of cells for the case of extensive fracture distribution, which leads to substantial computational costs. In this work, we use an embedded fractured model (EFM) that allows constructing mesh for fracture networks independently of porous media mesh [28–30]. However, a detailed fine grid is still required for a heterogeneous porous media with high contrast coefficients [31–33].

One way to solve this problem is to solve the problem on a coarse grid [34–36]. In this study, we use multiscale modeling techniques to reduce the dimensionality of the original problem [37–39]. There are many modifications of multiscale methods where each may suit a specific task. The most famous is the multiscale finite element method (MsFEM) [37,39,40]. The MsFEM can give a significant error in domains with high-contrast properties. The Generalized Multiscale Finite Element Method (GMsFEM) is based on the spectral properties of the local problem and provides accurate approximation by defining multiple basis functions in local domains [41–45]. Based on the finite volume method, a multiscale finite volume method (MsFVM) was developed [46,47]. The mixed finite element method (Mixed-FEM) has been developed to solve fluid flow problems in porous media [48–51]. Multiscale methods with an oversampling strategy are used for problems with complex heterogeneity, such as channels or fractures. In the constraint energy minimizing generalized multiscale finite element method (CEM-GMsFEM), the multiscale basis functions are constructed in oversampled local domains and therefore take into account the influence of heterogeneity in neighboring local domains [52–57]. For nonlinear problems, the online generalized multiscale finite method (Online GMsFEM) can be used where additional multiscale bases take into account changes in properties in nonlinear problems [58–61]. In our previous work [62], we used the mixed generalized finite element method for the Darcy-Forchheimer model in a heterogeneous domain. This paper extends the Darcy-Forchheimer model by adding fractures and time. As a multiscale method, we chose the non-local multicontinuum method (NLMC) [54,63,64].

In this paper, we look at a non-local multicontinuum method (NLMC) for Darcy-Forchheimer flow in a fractured domain. The algorithm is divided into two parts: offline and online stages. In the offline stage, we

construct multiscale basis functions. In this algorithm, we calculate bases in oversampled local domains with energy-minimizing constraints. At the online step, using the acquired bases, we solve the system on a coarse grid. It should be noted that the approximation relies on the finite volume method, and that fractures are represented by an embedded fracture model of lower dimensional fractures. Numerical results are presented for a two-dimensional fractured heterogeneous domain. The numerical experiment comprises examining the accuracy of the NLMC approach in relation to nonlinearity.

The Darcy-Forchheimer model is shown in a fractured heterogeneous domain in Section 2. A fine grid approximation using the finite volume method and embedded fracture model (EFM) is described in Section 3. The non-local multicontinuum technique (NLMC) algorithm for the Darcy-Forchheimer model is presented in Section 4. We describe multiscale basis functions in oversampled domains with constraints. In Section 5, we analyse the impact of nonlinearity on the method's accuracy and offer a numerical experiment for two test scenarios.

2 Problem formulation

The filtration process is described by the well-known Darcy law equation:

$$\mu k^{-1} \mathbf{u} + \nabla p = 0. \quad (1)$$

Let us supplement the basic equation of Darcy's law with a nonlinear term. The nonlinear Darcy-Forchheimer equation writing as follows:

$$\mu k^{-1} \mathbf{u} + \rho \beta |\mathbf{u}| \mathbf{u} + \nabla p = 0, \quad (2)$$

where p is the pressure, \mathbf{u} is the velocity, k is the heterogeneous permeability, μ is the viscosity, ρ is the density and β is the Forchheimer coefficient. The impact of nonlinearity on the overall physical process is determined by the Forchheimer coefficient.

We can express the equation (2) as:

$$\mathbf{u} = -\frac{k/\mu}{1 + \rho \beta k |\mathbf{u}|/\mu} \nabla p. \quad (3)$$

In this study, we take a dynamic nonlinear filtration process into consideration and include a temporal derivative

$$\frac{\partial(\rho \phi)}{\partial t} + \nabla \cdot (\rho \mathbf{u}) = \rho f. \quad (4)$$

Assuming ρ as the constant, we set

$$\frac{\partial \phi}{\partial t} = c_r \phi_0 \frac{\partial p}{\partial t}, \quad c_r = \frac{1}{\phi_0} \frac{\partial \phi}{\partial p}, \quad c = c_r \phi_0, \quad (5)$$

where ϕ is the porosity and c_r is the porous media compressibility coefficient.

Therefore, the dynamic incompressible single-phase Darcy-Forchheimer flow equation can be written as follows:

$$c \frac{\partial p}{\partial t} + \nabla \cdot \mathbf{u} = f, \quad (6)$$

where f is a source term.

In this paper, we consider the nonlinear filtration process in fractured media. We define the porous matrix domain as $\Omega \in \mathcal{R}^d$ and lower dimensional fractures as $\gamma \in \mathcal{R}^{d-1}$. In our implementation, we consider problems in the two-dimensional domain $d = 2$. We consider the problem in fractured media using the following model:

$$\begin{aligned} c_m \frac{\partial p_m}{\partial t} + \nabla \cdot \mathbf{u}_m + r_{mf}(p_m, p_f) &= f_m, & \mathbf{x} \in \Omega, & \quad t > 0 \\ c_f \frac{\partial p_f}{\partial t} + \nabla \cdot \mathbf{u}_f - r_{mf}(p_m, p_f) &= f_f, & \mathbf{x} \in \gamma, & \quad t > 0 \end{aligned} \quad (7)$$

where m and f denotes subindices for matrix and fracture, r_{mf}, r_{fm} are the transfer terms between matrix-fracture and fracture-matrix.

From (3) for the velocity \mathbf{u}_i , we have

$$\mathbf{u}_i = -\frac{k_i/\mu}{1 + \rho\beta_i k_i |\mathbf{u}_i|/\mu} \nabla p_i, \quad i = m, f. \quad (8)$$

Finally, the nonlinear Darcy-Forchheimer flow in a fractured domain is defined by the following coupled system of equations

$$\begin{aligned} c_m \frac{\partial p_m}{\partial t} - \nabla \cdot \left(\frac{k_m/\mu}{1 + \rho\beta_m k_m |\mathbf{u}_m|/\mu} \nabla p_m \right) + r_{mf}(p_m, p_f) &= f_m, & \mathbf{x} \in \Omega, & \quad t > 0 \\ c_f \frac{\partial p_f}{\partial t} - \nabla \cdot \left(\frac{k_f/\mu}{1 + \rho\beta_f k_f |\mathbf{u}_f|/\mu} \nabla p_f \right) - r_{mf}(p_m, p_f) &= f_f, & \mathbf{x} \in \gamma, & \quad t > 0. \end{aligned} \quad (9)$$

We supplement the equation (9) with the following boundary conditions

$$\mathbf{u}_m \cdot \mathbf{n} = 0, \quad \mathbf{u}_f \cdot \mathbf{n} = 0, \quad \mathbf{x} \in \partial\Omega, \quad t > 0, \quad (10)$$

and given initial condition $p_m = p_f = p_0$ for $t = 0$.

3 Fine grid approximation

Next, we consider the fine grid approximation of the problem (9), (10). We use the finite volume method with an embedded fracture model. We define structured triangular fine grid \mathcal{T}_h , which does not conform to fractures. We build a separate mesh for fractures and denote it as \mathcal{E}_h . For the time-dependent problem, we note n as a number of time layers, τ as the time step, and $T_{max} = n\tau$ as the final time. To make an approximation of the fine grid, we define the element of the fine grid ς_i and the element of fracture mesh u_l . We consider N_f^m and N_f^f as the number of elements in fine grids of matrix and fracture, respectively. From that, we can write a fine grid for porous matrix domain as $\mathcal{T}_h = \bigcup_{i=1}^{N_f^m} \varsigma_i$ and for fractures as $\mathcal{E} = \bigcup_{l=1}^{N_f^f} u_l$.

We have the following approximation on the fine grid:

$$\begin{aligned} c_m \frac{p_{m,i}^{n+1} - p_{m,i}^n}{\tau} |\varsigma_i| + \sum_j T_{ij}^n (p_{m,i}^{n+1} - p_{m,j}^{n+1}) + \sum_l \sigma_{il}^n (p_{m,i}^{n+1} - p_{f,l}^{n+1}) &= f_{m,i} |\varsigma_i|, \quad \forall i = 1, N_f^m, \\ c_f \frac{p_{f,l}^{n+1} - p_{f,l}^n}{\tau} |u_l| + \sum_\eta W_{l\eta}^n (p_{f,l}^{n+1} - p_{f,\eta}^{n+1}) - \sum_i \sigma_{il}^n (p_{m,i}^{n+1} - p_{f,l}^{n+1}) &= f_{f,l} |u_l|, \quad \forall l = 1, N_f^f, \end{aligned} \quad (11)$$

with

$$T_{ij}^n = Z_{ij} \varrho_{ij}^n, \quad \text{where} \quad Z_{ij} = \frac{k_{m,ij} |E_{ij}|}{\mu d_{ij}^m}, \quad \varrho_{ij}^n = \frac{1}{1 + \rho \beta_{m,ij} k_{m,ij} |u_{m,ij}^n| / \mu},$$

$$W_{l\eta}^n = X_{l\eta} w_{l\eta}^n \quad \text{where} \quad X_{l\eta} = \frac{k_{f,l\eta}}{\mu d_{l\eta}^f}, \quad w_{l\eta}^n = \frac{1}{1 + \rho \beta_{f,l\eta} k_{f,l\eta} |u_{f,l\eta}^n| / \mu},$$

where

$$k_{m,ij} = \frac{2}{1/k_{m,i} + 1/k_{m,j}}, \quad \beta_{m,ij} = \frac{2}{1/\beta_{m,i} + 1/\beta_{m,j}},$$

$$k_{f,l\eta} = \frac{2}{1/k_{f,l} + 1/k_{f,\eta}}, \quad \beta_{f,l\eta} = \frac{2}{1/\beta_{f,l} + 1/\beta_{f,\eta}},$$

and $|E_{ij}|$ is the length of facet between cells ς_i and ς_j , d_{ij} is the distance between midpoint of cells ς_i and ς_j , and $d_{l\eta}^f$ is the distance between midpoint of cells ι_l and ι_η .

For transfer terms, we use the following approximation

$$\sigma_{il}^n = Y_{il} \bar{\vartheta}_{il}, \quad \text{where} \quad Y_{il} = \frac{k_{il}^* |\gamma_{il}|}{\mu \theta_{il}}, \quad \bar{\vartheta}_{il} = \frac{1}{1 + \rho \beta_{il}^* k_{il}^* |u_{mf,il}^n| / \mu},$$

where

$$k_{il}^* = \frac{2}{1/k_{m,i} + 1/k_{f,l}}, \quad \beta_{il}^* = \frac{2}{1/\beta_{m,i} + 1/\beta_{f,l}},$$

and $C_{il} = \frac{|\gamma_{il}|}{\theta_{il}}$ is the connectivity index, θ_{il} is the distance midpoint of matrix cell ς_i and fracture cell ι_l , $|\gamma_{il}|$ is the length of the intersection of the fractures cell ι_l and matrix cell ς_i .

Therefore, we can present the system of equations (11) in matrix form:

$$M \frac{p^{n+1} - p^n}{\tau} + (A^n + Q^n) p^{n+1} = F, \quad \mathbf{x} \in \Omega, \quad (12)$$

where

$$M = \begin{pmatrix} M_m & 0 \\ 0 & M_f \end{pmatrix}, \quad A^n = \begin{pmatrix} A_m^n & 0 \\ 0 & A_f^n \end{pmatrix}, \quad Q^n = \begin{pmatrix} Q_{mf}^n & -Q_{mf}^n \\ -Q_{fm}^n & Q_{fm}^n \end{pmatrix}, \quad F = \begin{pmatrix} F_m \\ F_f \end{pmatrix},$$

and

$$M_m = \{m_{ij}^m\}, \quad m_{ij}^m = \begin{cases} c_m |\varsigma_i| & i = j, \\ 0 & i \neq j \end{cases}, \quad M_f = \{m_{l\eta}^f\}, \quad m_{l\eta}^f = \begin{cases} c_f |\iota_l| & l = \eta, \\ 0 & l \neq \eta \end{cases},$$

$$A_m^n = \{a_{ij}^{m,n}\}, \quad a_{ij}^{m,n} = \begin{cases} \sum_j T_{ij}^n & i = j, \\ -T_{ij}^n & i \neq j \end{cases}, \quad A_f^n = \{a_{l\eta}^{f,n}\}, \quad a_{l\eta}^{f,n} = \begin{cases} \sum_\eta W_{l\eta}^n & l = \eta, \\ -W_{l\eta}^n & l \neq \eta \end{cases}, \quad (13)$$

$$Q_{fm}^n = \{q_{il}^{fm,n}\}, \quad q_{ij}^{fm,n} = \begin{cases} \sigma_{li}^n & \iota_l \subset \varsigma_i, \\ 0 & l \neq \eta \end{cases}, \quad Q_{mf}^n = (Q_{fm}^n)^T,$$

In this approximation, we have nonlinear terms T_{ij}^n , $W_{l\eta}^n$ and σ_{li}^n that can be factorized to the linear part Z_{ij} , $X_{l\eta}$, Y_{il} and nonlinear part ϱ_{ij}^n , $w_{l\eta}^n$, $\bar{\vartheta}_{il}$. We use the nonlinear velocity \mathbf{u}_m and \mathbf{u}_f from the previous time layer.

4 Coarse grid approximation

Next, we present a coarse grid approximation using the Non-Local Multi-Continuum method (NLMC). In this approach, we construct the multiscale basis functions in an oversampled local domain. To derive the multiscale basis function, we solve local problems with constraints. Each multiscale basis is calculated for one target continuum, determined by the imposed constraints. Multiscale basis functions use a constraint that makes an integral over the local domain (coarse cell) disappear in all continuums besides the target continuum and provide a meaning of the coarse grid solution. The basis functions were calculated for each fracture network rather than for each fracture individually. Such an approach of basis construction separates background and fractures and has spatial decay properties.

Let \mathcal{T}_H be the coarse grid divided into coarse cells K_i . We define an oversampled local domain K_i^+ by increasing K_i by several coarse oversampling layers. We denote the number of oversampling layers as S . An example of local domains K_i^+ with a different number of oversampling layers is presented in Figure 1. The fracture network $\gamma^{(l)}$ connects into global fracture network $\gamma = \cup_{l=1}^L \gamma^{(l)}$, where L is the total number of fracture networks in K_i . In each coarse cell K_j we have L_j amount of fracture network and $\gamma_j^{(l)} = K_j \cap \gamma^{(l)}$ is the fracture network laying inside K_j . In each coarse cell K_i , we construct $L_i + 1$ multiscale basis functions: L_i functions for each fracture network $\gamma_i^{(l)}$ and one for background medium K_i .

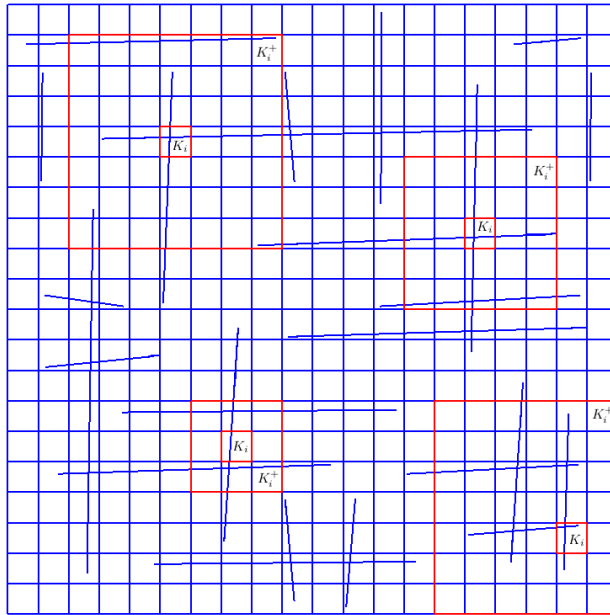


Figure 1: Coarse grid with local domains K_i^+ and different numbers of oversampling layers.

The NLMC method is divided into two stages: offline and online. In the offline stage, we construct the multiscale basis functions. We solve a system on the coarse grid using multiscale basis functions in the online stage. To derive the multiscale basis functions, we solve the following problem in each oversampled local

domain K_i^+ :

$$\begin{aligned}\nabla \cdot \left(\frac{k_m}{\mu} \nabla \psi_m^i \right) + \tilde{r}_{mf} (\psi_m^i - \psi_f^i) &= 0, \\ \nabla \cdot \left(\frac{k_f}{\mu} \nabla \psi_f^i \right) - \tilde{r}_{mf} (\psi_m^i - \psi_f^i) &= 0,\end{aligned}\tag{14}$$

with

$$\psi_m^i = 0, \quad \psi_f^i = 0, \quad \mathbf{x} \in \partial K_i^+.$$

Here we use a linear part of transfer term r_{mf} , which will be explained further below.

We apply the following constraints for the problem (14) in each $K_j \subset K_i^+$:

- for background:

$$\frac{1}{|K_j|} \int_{K_j} \psi_m^{i,0} dx = \delta_{i,j}, \quad \frac{1}{|\gamma_j^{(m)}|} \int_{\gamma_j^{(m)}} \psi_f^{i,0} ds = 0, \quad m = \overline{1, L_j},\tag{15}$$

- for fractures:

$$\frac{1}{|K_j|} \int_{K_j} \psi_m^{i,l} dx = 0, \quad \frac{1}{|\gamma_j^{(m)}|} \int_{\gamma_j^{(m)}} \psi_f^{i,l} ds = \delta_{i,j} \delta_{m,l}, \quad m, l = \overline{1, L_j},\tag{16}$$

with $\psi^{i,l} = (\psi_m^{i,0}, \psi_f^{i,0})$ and $\psi^{i,l} = (\psi_m^{i,l}, \psi_f^{i,l})$.

The constraints provide a function for background medium that has a mean value of one in K_i and a mean value of zero elsewhere in K_i^+ . Additionally, all fractures inside the oversampled local domain K_i^+ will have mean values of one for the multiscale basis function. We have a basis function for the fracture network in the background continuum that has a mean value of zero for each coarse cell in K_i^+ . Moreover, for the target fracture network $\gamma_i^{(l)}$, we have basis functions with mean values one and zero for all fracture networks inside K_i^+ .

We should mention that we compute multiscale basis functions for the linear parts of T_{ij} and $W_{l\eta}$ from (11). The multiscale basis functions were computed only once and did not vary over time. Therefore, the approximation of the problem (14) takes the following form:

$$\begin{aligned}\sum_j Z_{kj} (\psi_{m,k}^{i,l} - \psi_{m,j}^{i,l}) + \sum_n Y_{kn} (\psi_{m,k}^{i,l} - \psi_{f,n}^{i,l}) &= 0, \quad \forall k = \overline{1, N_{f,K_i^+}^m} \\ \sum_\eta X_{l\eta} (\psi_{f,n}^{i,l} - \psi_{f,\eta}^{i,l}) - \sum_k Y_{il} (\psi_{m,k}^{i,l} - \psi_{f,n}^{i,l}) &= 0, \quad \forall n = \overline{1, N_{f,K_i^+}^f}.\end{aligned}\tag{17}$$

In approximation (17), all notations are taken from (11), except $N_{f,K_i^+}^m$ and $N_{f,K_i^+}^f$, which represent the number of fine grids elements in oversampled local domain K_i^+ . The approximation of the local problem for the development of multiscale basis functions can be represented in the matrix form:

$$\begin{pmatrix} A_m^i + Q_{mf}^i & -Q_{mf}^i & (B_m^i)^T & 0 \\ -Q_{fm}^i & A_f^i + Q_{fm}^i & 0 & (B_f^i)^T \\ B_m^i & 0 & 0 & 0 \\ 0 & B_f^i & 0 & 0 \end{pmatrix} \begin{pmatrix} \psi_m^{i,l} \\ \psi_f^{i,l} \\ \varphi_m^{i,l} \\ \varphi_f^{i,l} \end{pmatrix} = \begin{pmatrix} 0 \\ 0 \\ F_m^{i,l} \\ F_f^{i,l} \end{pmatrix},\tag{18}$$

where φ_m^i and φ_f^i are Lagrange multipliers, that comes from constraints. For matrix continuum (first basis) we set $F_m^{i,0} = \{f_{m,j}^{i,0}\}$, $f_{m,j}^{i,0} = \delta_{i,j}$ and $F_f^{i,0} = \mathbf{0}$. For m th fracture we set $F_m^{i,l} = \mathbf{0}$ and $F_f^{i,l} = \{f_{f,j}^{i,l}\}$, $f_{f,j}^{i,l} = \delta_{i,j}\delta_{m,l}$. Figure 2 demonstrates an illustration of multiscale basis functions that was computed in K_i^+ using four oversampling layers.

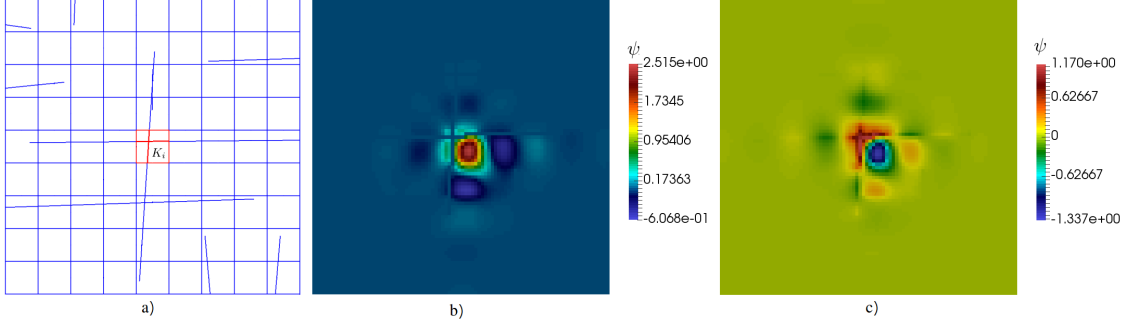


Figure 2: a) Oversampled local domain K_i^+ . b) Multiscale basis function for matrix c) Multiscale basis function for fracture network.

Next, we can define the multiscale space using obtained multiscale basis functions:

$$V_{ms} = \text{span}\{(\psi_m^{i,l}, \psi_f^{i,l}), i = \overline{1, N_c}, l = \overline{0, L_i}\}. \quad (19)$$

To solve the problem on the coarse grid, we define a projection matrix on multiscale space:

$$R = \begin{pmatrix} R_{mm} & R_{mf} \\ R_{fm} & R_{ff} \end{pmatrix}, \quad (20)$$

$$R_{mm} = [\psi_m^{0,0}, \psi_m^{1,0}, \dots, \psi_m^{N_c,0}]^T, \quad R_{ff} = [\psi_f^{0,1}, \dots, \psi_f^{0,L_0}, \psi_f^{1,1}, \dots, \psi_f^{1,L_1}, \dots, \psi_f^{N_c,1}, \dots, \psi_f^{N_c,L_{N_c}}]^T,$$

$$R_{fm} = [\psi_m^{0,1}, \dots, \psi_m^{0,L_0}, \psi_m^{1,1}, \dots, \psi_m^{1,L_1}, \dots, \psi_m^{N_c,1}, \dots, \psi_m^{N_c,L_{N_c}}]^T, \quad R_{mf} = [\psi_f^{0,0}, \psi_f^{1,0}, \dots, \psi_f^{N_c,0}]^T.$$

Next, we write approximation on the coarse grid for $\bar{p}^{n+1} = (\bar{p}_m^{n+1}, \bar{p}_f^{n+1})^T$

$$\bar{M} \frac{\bar{p}^{n+1} - \bar{p}^n}{\tau} + (\bar{A}^n + \bar{Q}^n) \bar{p}^{n+1} = \bar{F}, \quad (21)$$

where

$$\bar{A}^n = RA^nR^T, \quad \bar{M} = RMR^T, \quad \bar{Q}^n = RQ^nR^T, \quad \bar{F} = RF. \quad (22)$$

The resulting functions \bar{p}_m^{n+1} and \bar{p}_f^{n+1} store the average values over the coarse grid element. In addition, we can reconstruct a solution on the fine grid by $p_{ms}^{n+1} = R^T \bar{p}^{n+1}$.

Finally, we can summarize the algorithm of the NLMC method as follows:

1. Define the coarse grid \mathcal{T}_H and oversampled local domains K_i^+ for a given number of oversampling layers.
2. Solve local problems (18) in each K_i^+ to get the multiscale basis functions;
3. Construct the projection matrix R by combining multiscale basis functions;
4. Project and solve the nonlinear system on the coarse grid (21).

5 Numerical results

In this section, we use NLMC to provide numerical results for the Darcy-Forchheimer problem. We consider the flow problem in the two-dimensional fractured heterogeneous domain. Figure 3 presents the computation domain with the fracture location. We present numerical results for two test cases with different heterogeneous coefficients k_m and denote test problems as *Test 1* and *Test 2*. We show the heterogeneous coefficient k_m in Figure 3. We chose a highly heterogeneous domain for *Test 2* with a significant contrast in k_m values inside one coarse cell K_i . For fractures, we set $k_f = 10^9$ to test both cases.

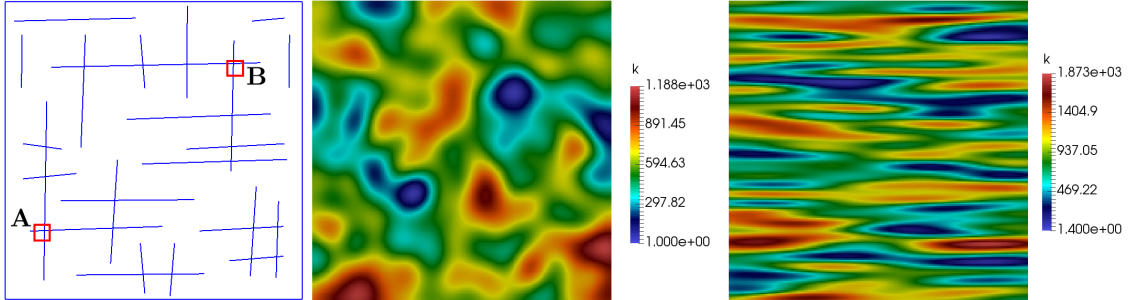


Figure 3: Heterogeneity and fracture distribution. Left: computational domain Ω with fractures γ . Middle: Coefficient k_m in *Test 1*. Right: Coefficient k_m in *Test 2*.

We consider numerical experiments for two coarse grids: 20×20 and 40×40 . Simulations are performed for $T_{max} = 12.5 \cdot 10^5$ with 100 time layers. The large number of time layers is used to resolve the nonlinearity using an approximation from the previous time layer. To investigate the accuracy of the NLMC algorithm, we compare the multiscale solutions with the reference solutions. We take a fine-grid solution as a reference solution. We use 200×200 uniform mesh with square cells for fine grid solution in a porous medium. For the fracture network, we use a one-dimensional mesh with 1730 elements. The fine grid system's size equals 41733×41733 . We compare solutions by using L_2 norm errors:

$$\|e\|_p^{L_2} = \sqrt{\frac{\int_{\Omega} (p_f - p_{ms})^2 dx}{\int_{\Omega} p_f^2 dx}}, \quad \|\bar{e}\|_p^{L_2} = \sqrt{\frac{\int_{\Omega} (\bar{p}_f - \bar{p}_{ms})^2 dx}{\int_{\Omega} \bar{p}_f^2 dx}}, \quad (23)$$

where p_{ms} is the multiscale solution, p_f is the solution on the fine grid, \bar{p}_{ms} , \bar{p}_f are the average values over the coarse grid element for multiscale and fine grid solutions, respectively.

We consider results with different values of β_i to investigate the effect of nonlinearity. In implementation, we set $\beta_m = Ck_m^{-1}$ and $\beta_f = Ck_f^{-1}$. We change the value of C to control the effect of nonlinearity. We consider results for $C = 10^4, 10^3, 10^2, 10, 0$. We set $\mu = 8$, $\rho = 1.0$, $c_m = c_f = 1.0$, $r_{mf} = k_m$, $f_m = 0$. The source term for fractures f_f contains two wells: injection and production. We put injection well in all fracture cells inside coarse cell **A** with $f_A = 10^{-3}$ and production well in all fracture cells inside coarse cell **B** with $f_B = -10^{-3}$. The location of injection and production wells are presented in Figure 3.

The numerical results for *Test 1* is presented in Figure 4 for $C = 10^4$. Figure 5 shows an solution on 40×40 coarse grid for *Test 1* with $C = 10^4$. The first row shows a solution on a fine grid, while the second

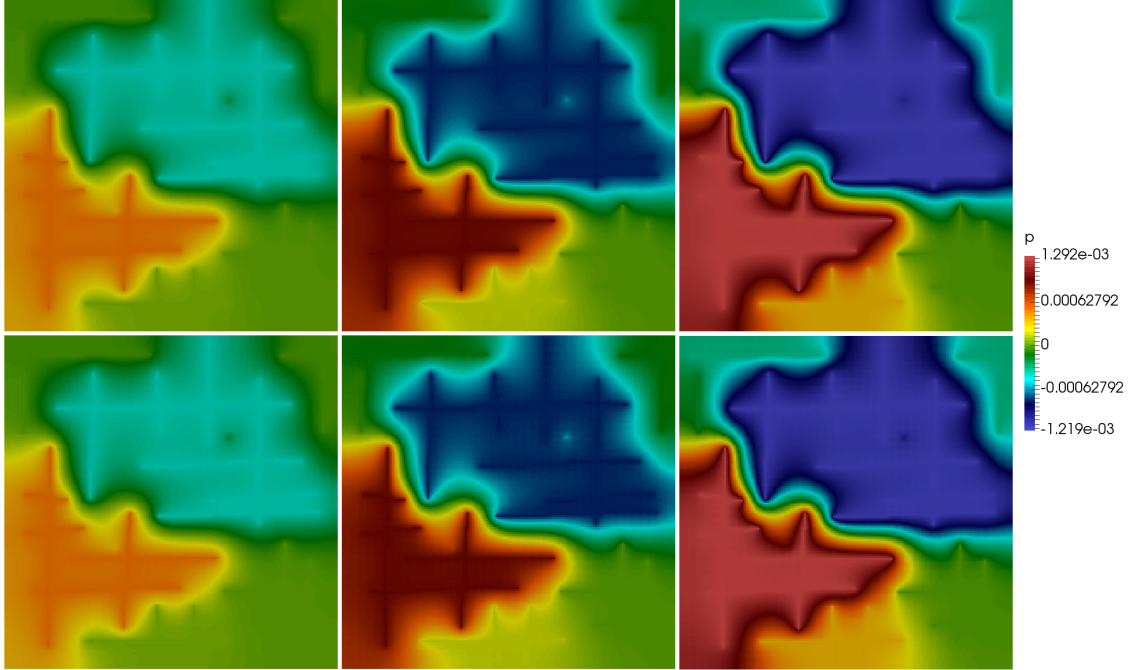


Figure 4: Numerical results for $C = 10^4$ at the 30th, 60th, and last time layer. First row: fine grid solution. Second row: NLMC-solution on 40×40 coarse grid using four oversampling layers. *Test 1*.

row shows a solution using NLMC with four oversampling layers in basis construction. We present solutions for the 30th, 60th, and final time layers to demonstrate time distribution. In the figures, the NLMC solution and the fine grid solution are looks similar.

For *Test 2*, we present results in Figure 6. Figure 7 shows solution on 40×40 coarse grid for *Test 2* with $C = 10^4$. The results are presented in the same order as *Test 1* for $C = 10^4$ and four oversampling layers in NLMC. We observe the same behavior as *Test 1*. The results are presented for the case with a larger influence of nonlinearity, $C = 10^4$.

S	20×20 Coarse grid		40×40 Coarse grid		S	20×20 Coarse grid		40×40 Coarse grid	
	$e_p^{L_2}, (\%)$	$\bar{e}_p^{L_2}, (\%)$	$e_p^{L_2}, (\%)$	$\bar{e}_p^{L_2}, (\%)$		$e_p^{L_2}, (\%)$	$\bar{e}_p^{L_2}, (\%)$	$e_p^{L_2}, (\%)$	$\bar{e}_p^{L_2}, (\%)$
3	6.583	6.337	5.576	5.364	3	8.165	7.922	6.674	6.643
4	0.826	0.345	0.693	0.403	4	0.944	0.487	0.751	0.503
5	0.179	0.017	0.144	0.029	5	0.198	0.026	0.144	0.036
6	0.039	0.001	0.035	0.001	6	0.046	0.001	0.035	0.001
7	0.014	0.001	0.009	0.001	7	0.013	0.001	0.009	0.001

Table 1: Numerical results for $C = 0$. Left: *Test 1*. Right: *Test 2*.

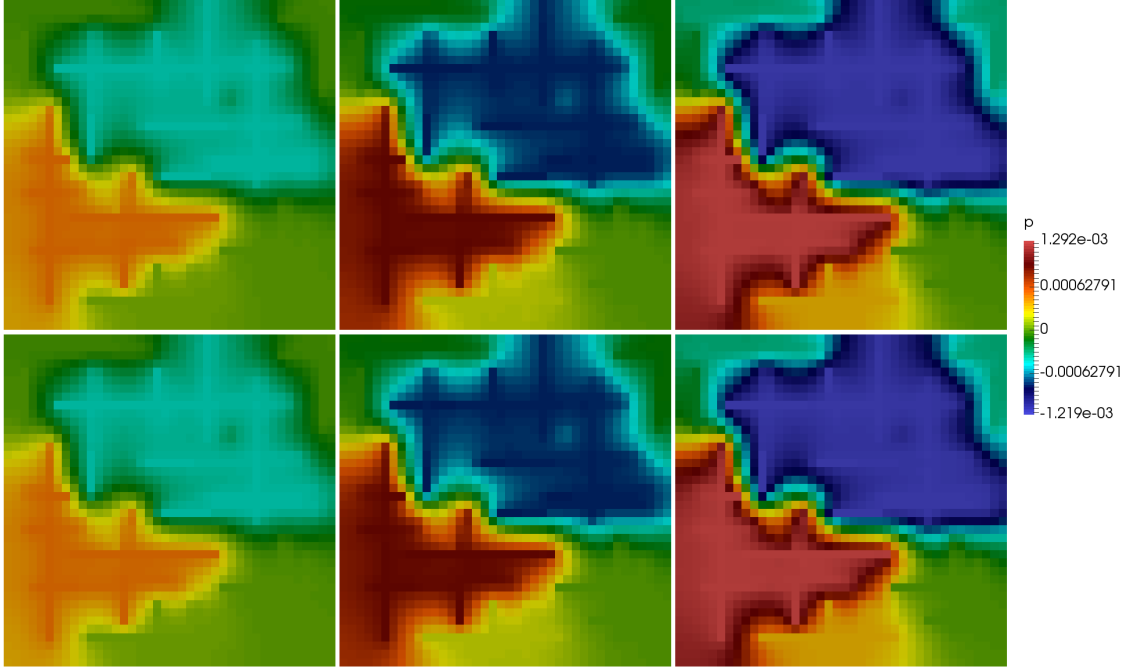


Figure 5: Numerical results for $C = 10^4$ at the 30th, 60th, and last time layer. First row: Coarse-grid average of the fine grid solution on 40×40 coarse grid. Second row: NLMC-solution on 40×40 coarse grid using four oversampling layers. *Test 1*.

S	20×20		40×40		S	20×20		40×40	
	Coarse grid		Coarse grid			Coarse grid		Coarse grid	
	$e_p^{L_2}, (\%)$	$\bar{e}_p^{L_2}, (\%)$	$e_p^{L_2}, (\%)$	$\bar{e}_p^{L_2}, (\%)$		$e_p^{L_2}, (\%)$	$\bar{e}_p^{L_2}, (\%)$	$e_p^{L_2}, (\%)$	$\bar{e}_p^{L_2}, (\%)$
3	6.583	6.338	5.577	5.365	3	8.165	7.923	6.674	6.643
4	0.826	0.345	0.693	0.403	4	0.944	0.487	0.749	0.503
5	0.179	0.017	0.144	0.029	5	0.198	0.026	0.144	0.036
6	0.039	0.001	0.035	0.001	6	0.046	0.001	0.035	0.001
7	0.014	0.001	0.009	0.001	7	0.013	0.001	0.009	0.001

Table 2: Numerical results for $C = 10$. Left: *Test 1*. Right: *Test 2*.

We present a relative L_2 error in Tables 1-5. We give results with varying numbers of oversampling layers, $S = 3, 4, 5, 6$ and 7 . In the left table, the errors for *Test 1* are presented. The results for *Test 2* are presented in the right table. In the tables, we demonstrate two errors: $e_2^{L_2}$ is the error on the fine grid and $\bar{e}_2^{L_2}$ is the error determined on the coarse grid. We consider accuracy for two coarse grids: 20×20 and 40×40 . The size of the coarse system is equal to 562×562 for 20×20 coarse grid and 1930×1930 for 40×40 coarse grid. We see that the size of the coarse system is smaller than the fine grid system discussed above. Moreover, we can see that employing four oversampling layers in all computations is enough to produce an accurate

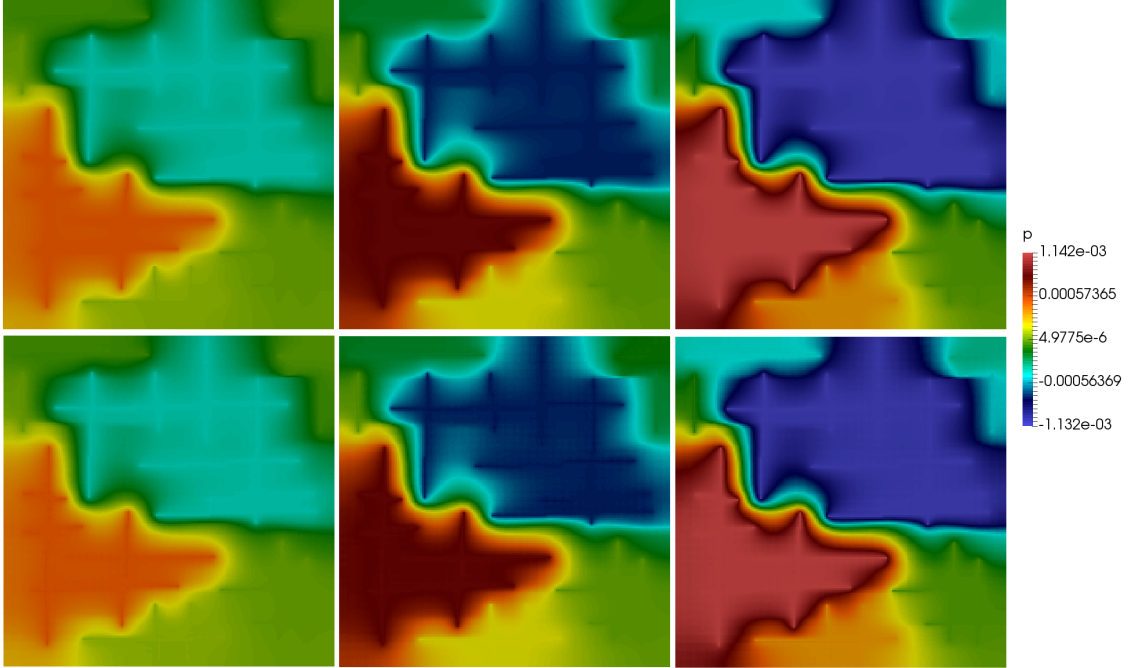


Figure 6: Numerical results for $C = 10^4$ at the 30th, 60th, and last time layers. First row: fine grid solution. Second row: NLMC-solution on 40×40 coarse grid using four oversampling layers. *Test 2*.

S	20×20		40×40		S	20×20		40×40	
	Coarse grid		Coarse grid			Coarse grid		Coarse grid	
	$e_p^{L_2}, (\%)$	$\bar{e}_p^{L_2}, (\%)$	$e_p^{L_2}, (\%)$	$\bar{e}_p^{L_2}, (\%)$		$e_p^{L_2}, (\%)$	$\bar{e}_p^{L_2}, (\%)$	$e_p^{L_2}, (\%)$	$\bar{e}_p^{L_2}, (\%)$
3	6.583	6.339	5.577	5.365	3	8.163	7.924	6.675	6.645
4	0.826	0.345	0.693	0.403	4	0.944	0.487	0.751	0.503
5	0.181	0.017	0.144	0.031	5	0.198	0.026	0.144	0.036
6	0.039	0.001	0.035	0.001	6	0.046	0.001	0.035	0.001
7	0.013	0.001	0.009	0.001	7	0.014	0.001	0.009	0.001

Table 3: Numerical results for $C = 10^2$. Left: *Test 1*. Right: *Test 2*.

solution. The solution diverges when we use 1 or 2 oversampling layers, and we did not include these results in the tables. The multiscale basis functions with three layers provide a solution with low accuracy. We have a small difference in error between *Test 1* and *Test 2*. We see that the difference in accuracy is greater when we employ a small number of oversampling layers. However, it becomes very small when we increase the number of oversampling layers. This points out that the NLMC method accuracy is practically independent of the type of heterogeneity. Also, we investigate the solution's accuracy to the equation's nonlinear part. We have a very small increase in error when we are raising the value of C , including linear case with $C = 0$.

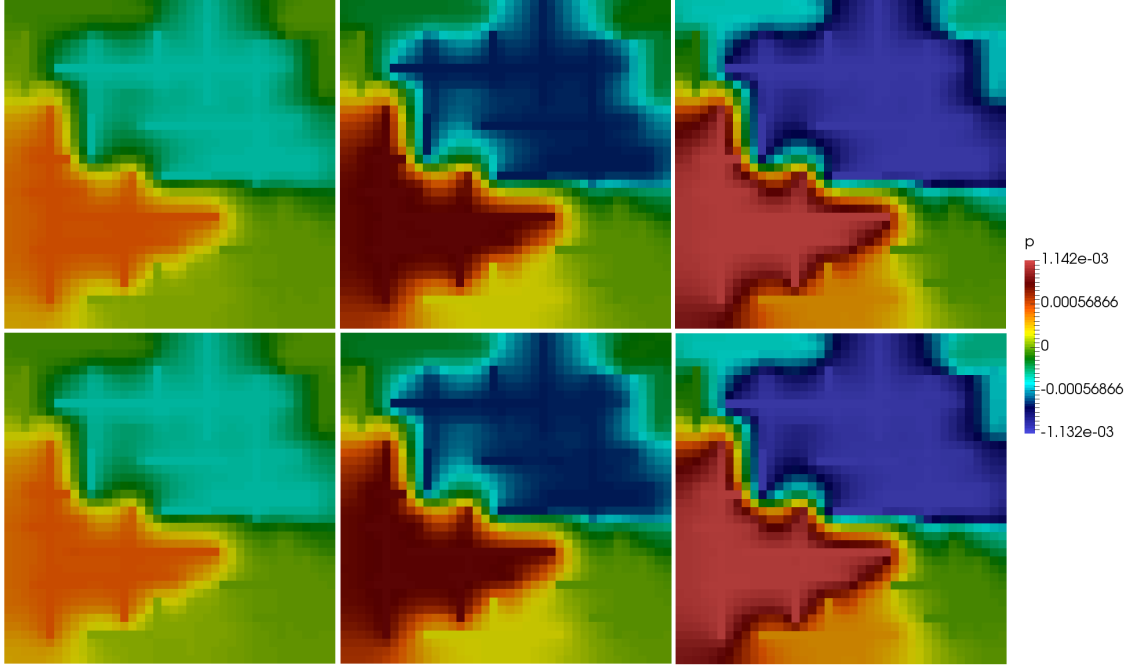


Figure 7: Numerical results for $C = 10^4$ at the 30th, 60th, and last time layers. First row: Coarse-grid average of the fine grid solution on 40×40 coarse grid. Second row: NLMC-solution on 40×40 coarse grid using four oversampling layers. *Test 2*.

S	20×20		40×40		S	20×20		40×40	
	Coarse grid		Coarse grid			Coarse grid		Coarse grid	
	$e_p^{L_2}, (\%)$	$\bar{e}_p^{L_2}, (\%)$	$e_p^{L_2}, (\%)$	$\bar{e}_p^{L_2}, (\%)$		$e_p^{L_2}, (\%)$	$\bar{e}_p^{L_2}, (\%)$	$e_p^{L_2}, (\%)$	$\bar{e}_p^{L_2}, (\%)$
3	6.584	6.349	5.582	5.372	3	8.145	7.935	6.684	6.659
4	0.826	0.346	0.693	0.403	4	0.944	0.489	0.751	0.503
5	0.179	0.017	0.144	0.029	5	0.199	0.026	0.144	0.036
6	0.039	0.001	0.035	0.001	6	0.047	0.001	0.035	0.001
7	0.015	0.001	0.009	0.001	7	0.015	0.001	0.009	0.001

Table 4: Numerical results for $C = 10^3$. Left: *Test 1*. Right: *Test 2*.

We can see a difference in error between $C = 10^4$ and $C = 10^3$, but the error is nearly similar in other values of C . It demonstrates that the NLMC only responds to large changes in nonlinearity, but it produces very good results even at bigger nonlinearity effects. We also analyze the method's accuracy to the coarse mesh size. The accuracy is better in coarse grid 40×40 than in coarse grid 20×20 .

To show the distribution of the error over time, we present graphs shown in Figure 8 and Figure 9. The graphs are constructed for $C = 10^4$ and contain the results for 3-7 oversampling layers. We get a significant

S	20×20 Coarse grid		40×40 Coarse grid		S	20×20 Coarse grid		40×40 Coarse grid	
	$e_p^{L_2}, (\%)$	$\bar{e}_p^{L_2}, (\%)$	$e_p^{L_2}, (\%)$	$\bar{e}_p^{L_2}, (\%)$		$e_p^{L_2}, (\%)$	$\bar{e}_p^{L_2}, (\%)$	$e_p^{L_2}, (\%)$	$\bar{e}_p^{L_2}, (\%)$
3	6.649	6.489	5.647	5.458	3	8.188	8.111	6.822	6.860
4	0.837	0.365	0.693	0.405	4	0.961	0.527	0.752	0.513
5	0.193	0.017	0.145	0.032	5	0.219	0.024	0.145	0.037
6	0.075	0.004	0.038	0.001	6	0.094	0.008	0.039	0.001
7	0.065	0.004	0.018	0.001	7	0.084	0.008	0.022	0.001

Table 5: Numerical results for $C = 10^4$. Left: *Test 1*. Right: *Test 2*.

error jump at the beginning with a coarse grid 20×20 . The error jump is small when we use a coarse grid of 40×40 . The error behavior became smooth after the beginning. We observe no error jumps throughout the process, keeping the error at the same level. We notice errors increasing throughout the simulation for three oversampling layers, which explains why we should employ four or more oversampling layers.

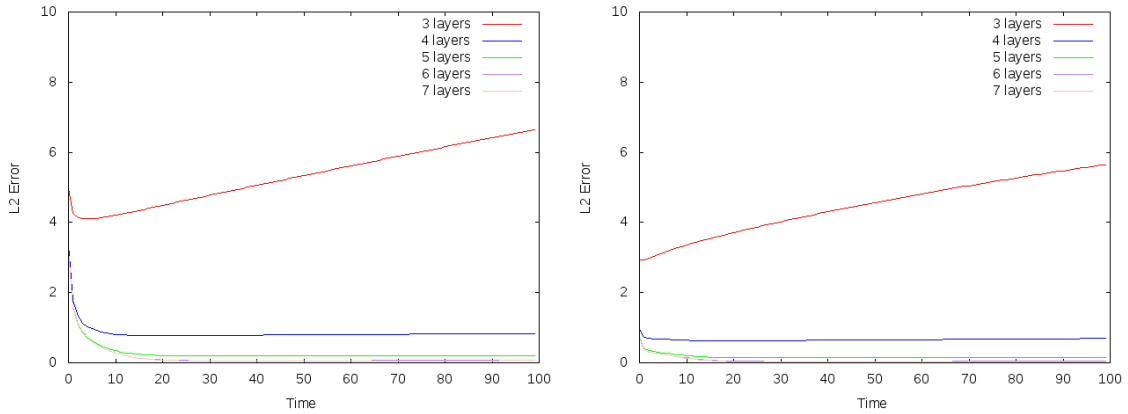


Figure 8: *Test 1*. Numerical results for $C = 10^4$. Relative L_2 error distribution in time. Left: 20×20 coarse grid. Right: 40×40 coarse grid.

We demonstrated that the presented NLMC algorithm gives highly accurate calculation results. Even in highly heterogeneous domains, the approach demonstrated great precision. The method’s accuracy is practically independent of the nonlinear part of the equation and the type of heterogeneity. We can improve accuracy by adding more oversampling layers. We observe that the method depends on the coarse grid’s size. The approach is more accurate on a finer coarse grid. Furthermore, the method significantly reduces the original system’s size. In our experiments, the coarse grid system size is significantly smaller than the fine grid system size (562×562 or 1930×1930 for the coarse grid and 41733×41733 for the fine grid). From this point, we can see that multiscale methods save computational resources, which is the primary advantage of multiscale methods over traditional mathematical modeling approaches.

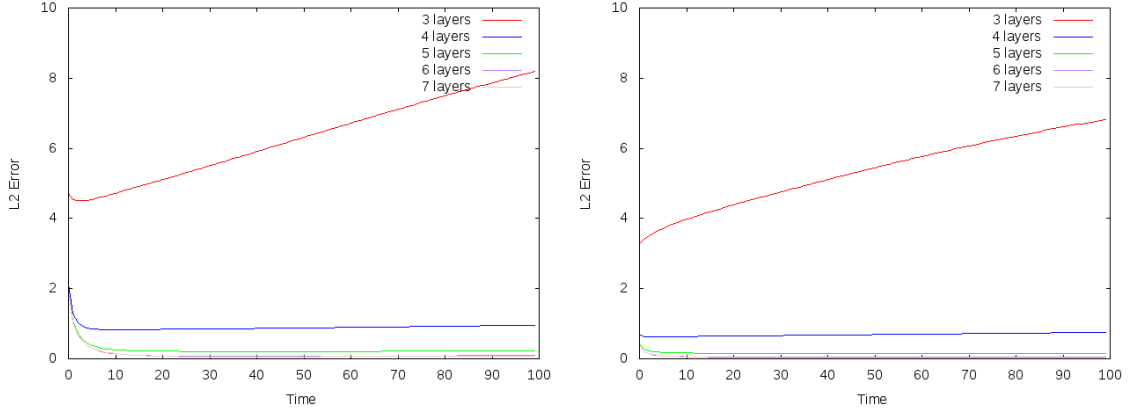


Figure 9: *Test 2*. Numerical results for $C = 10^4$. Relative L_2 error distribution in time. Left: 20×20 coarse grid. Right: 40×40 coarse grid.

6 Conclusion

This paper presented a Non-Local Multi-Continuum method (NLMC) algorithm for the time-dependent Darcy-Forchheimer model in a fractured heterogeneous domain. The fine grid approximation was constructed using the Finite volume method with a lower dimensional embedded fracture model. Model and methods formulations were given for two-dimensional cases. We completed a numerical experiment including two test cases with different heterogeneous properties. The numerical results are obtained for varying numbers of oversampling layers. We investigated nonlinearity’s impact by varying the coefficient β . The numerical experiment showed that the proposed approach had provided accurate results without significant influence of the nonlinear part of the flow. The performed numerical experiment showed good accuracy of the method. We conclude that the Non-Local Multi-Continuum technique performed well in modeling the Darcy-Forchheimer model in the fractured medium.

7 Acknowledgements

D. Spiridonov work is supported the grant of Russian Science Foundation No. 21-71-00061(<https://rscf.ru/en/project/21-71-00061/>) and the Russian government project Science and Universities (project No. FSRG-2021-0015) aimed at supporting junior laboratories.

References

- [1] Anna Cescon and Jia-Qian Jiang. Filtration process and alternative filter media material in water treatment. *Water*, 12(12):3377, 2020.

- [2] GC Maitland. Oil and gas production. *Current opinion in colloid & interface science*, 5(5-6):301–311, 2000.
- [3] P Schofield et al. Gas production methods. *Farm animal metabolism and nutrition*, pages 209–232, 2000.
- [4] L D’alpaos and A Defina. Mathematical modeling of tidal hydrodynamics in shallow lagoons: A review of open issues and applications to the venice lagoon. *Computers & Geosciences*, 33(4):476–496, 2007.
- [5] S He, Y Li, and RZ Wang. Progress of mathematical modeling on ejectors. *Renewable and Sustainable Energy Reviews*, 13(8):1760–1780, 2009.
- [6] K-J Reite and Asgeir J Sorensen. Mathematical modeling of the hydrodynamic forces on a trawl door. *IEEE Journal of oceanic Engineering*, 31(2):432–453, 2006.
- [7] Uygulaana S Gavrilieva, Valentin N Alekseev, and Mariya Vasil’evna Vasil’eva. Flow and transport in perforated and fractured domains with robin boundary conditions. *Mathematical notes of NEFU*, 24(3):65–77, 2017.
- [8] VI Vasil’ev, MV Vasil’eva, VS Gladkikh, VP Ilin, D Ya Nikiforov, DV Perevozkin, and GA Prokop’ev. Numerical solution of a fluid filtration problem in a fractured medium by using the domain decomposition method. *Journal of Applied and Industrial Mathematics*, 12:785–796, 2018.
- [9] DY Nikiforov and SP Stepanov. Numerical simulation of the embedded discrete fractures by the finite element method. In *Journal of Physics: Conference Series*, volume 1158, page 032038. IOP Publishing, 2019.
- [10] SL Lee and JH Yang. Modeling of darcy-forchheimer drag for fluid flow across a bank of circular cylinders. *International journal of heat and mass transfer*, 40(13):3149–3155, 1997.
- [11] M Ijaz Khan, Faris Alzahrani, and Aatef Hobiny. Simulation and modeling of second order velocity slip flow of micropolar ferrofluid with darcy–forchheimer porous medium. *Journal of Materials Research and Technology*, 9(4):7335–7340, 2020.
- [12] Yuming Chu, MI Khan, MIU Rehman, S Kadry, S Qayyum, and M Waqas. Stability analysis and modeling for the three-dimensional darcy-forchheimer stagnation point nanofluid flow towards a moving surface. *Applied Mathematics and Mechanics*, 42(3):357–370, 2021.
- [13] Maria Vasilyeva. Efficient decoupling schemes for multiscale multicontinuum problems in fractured porous media. *arXiv preprint arXiv:2209.01158*, 2022.
- [14] Vivette Girault and Mary F Wheeler. Numerical discretization of a darcy–forchheimer model. *Numerische Mathematik*, 110(2):161–198, 2008.
- [15] Klaus-Jürgen Bathe. Finite element method. *Wiley encyclopedia of computer science and engineering*, pages 1–12, 2007.

- [16] Gouri Dhatt, Emmanuel Lefrançois, and Gilbert Touzot. *Finite element method*. John Wiley & Sons, 2012.
- [17] Vishal Jagota, Aman Preet Singh Sethi, and Khushmeet Kumar. Finite element method: an overview. *Walailak Journal of Science and Technology (WJST)*, 10(1):1–8, 2013.
- [18] José J Salas, Hilda López, and Brígida Molina. An analysis of a mixed finite element method for a darcy–forchheimer model. *Mathematical and Computer Modelling*, 57(9-10):2325–2338, 2013.
- [19] Jian Huang, Long Chen, and Hongxing Rui. Multigrid methods for a mixed finite element method of the darcy–forchheimer model. *Journal of scientific computing*, 74:396–411, 2018.
- [20] Wenwen Xu, Dong Liang, and Hongxing Rui. A multipoint flux mixed finite element method for the compressible darcy–forchheimer models. *Applied Mathematics and Computation*, 315:259–277, 2017.
- [21] Robert Eymard, Thierry Gallouët, and Raphaële Herbin. Finite volume methods. *Handbook of numerical analysis*, 7:713–1018, 2000.
- [22] Fadl Moukalled, Luca Mangani, Marwan Darwish, F Moukalled, L Mangani, and M Darwish. *The finite volume method*. Springer, 2016.
- [23] Timothy Barth and Mario Ohlberger. *Finite volume methods: foundation and analysis*. 2003.
- [24] Mohammad Karimi-Fard and Louis J Durlofsky. Detailed near-well darcy-forchheimer flow modeling and upscaling on unstructured 3d grids. In *SPE Reservoir Simulation Symposium*. OnePetro, 2009.
- [25] Jérôme Jaffré, Mokhles Mnejja, and Jean E Roberts. A discrete fracture model for two-phase flow with matrix-fracture interaction. *Procedia Computer Science*, 4:967–973, 2011.
- [26] Mariya Vasil’evna Vasil’eva, Vasilii Ivanovich Vasiliev, Aleksei Andreevich Krasnikov, and D’ulustan Yakovlevich Nikiforov. Numerical simulation of single-phase fluid flow in fractured porous media. *Uchenye Zapiski Kazanskogo Universiteta. Seriya Fiziko-Matematicheskije Nauki*, 159(1):100–115, 2017.
- [27] T’T Garipov, M Karimi-Fard, and HA Tchelepi. Discrete fracture model for coupled flow and geomechanics. *Computational Geosciences*, 20:149–160, 2016.
- [28] Denis A Spiridonov and Mariya Vasil’evna Vasil’eva. Simulation of filtration problems in fractured porous media with mixed finite element method (embedded fracture model). *Mathematical notes of NEFU*, 24(3):100–110, 2017.
- [29] Mahmood Shakiba and Kamy Sepehrnoori. Using embedded discrete fracture model (edfm) and microseismic monitoring data to characterize the complex hydraulic fracture networks. In *SPE annual technical conference and exhibition*. OnePetro, 2015.

- [30] Aleksei Tyrylgin, Maria Vasilyeva, and Eric T Chung. Embedded fracture model in numerical simulation of the fluid flow and geo-mechanics using generalized multiscale finite element method. In *Journal of Physics: Conference Series*, volume 1392, page 012075. IOP Publishing, 2019.
- [31] Maria Vasilyeva, Wing T Leung, Eric T Chung, Yalchin Efendiev, and Mary Wheeler. Learning macroscopic parameters in nonlinear multiscale simulations using nonlocal multicontinua upscaling techniques. *Journal of Computational Physics*, 412:109323, 2020.
- [32] Maria Vasilyeva and Aleksey Tyrylgin. Machine learning for accelerating macroscopic parameters prediction for poroelasticity problem in stochastic media. *Computers & Mathematics with Applications*, 84:185–202, 2021.
- [33] Maria Vasilyeva, Aleksei Tyrylgin, Donald L Brown, and Anirban Mondal. Preconditioning markov chain monte carlo method for geomechanical subsidence using multiscale method and machine learning technique. *Journal of Computational and Applied Mathematics*, 392:113420, 2021.
- [34] Vasilii Grigoriev, Petr Zakharov, and Mir Akimov. Effective calculation of thermophysical properties of composite materials with multiple configurations by asymptotic homogenization technique. In *Journal of Physics: Conference Series*, volume 1392, page 012069. IOP Publishing, 2019.
- [35] Sergei Stepanov, Denis Spiridonov, and Tina Mai. Prediction of numerical homogenization using deep learning for the richards equation. *Journal of Computational and Applied Mathematics*, 424:114980, 2023.
- [36] A Tyrylgin, D Spiridonov, and M Vasilyeva. Numerical homogenization for poroelasticity problem in heterogeneous media. In *Journal of Physics: Conference Series*, volume 1158, page 042030. IOP Publishing, 2019.
- [37] Yalchin Efendiev and Thomas Y Hou. *Multiscale finite element methods: theory and applications*, volume 4. Springer Science & Business Media, 2009.
- [38] Grégoire Allaire and Robert Brizzi. A multiscale finite element method for numerical homogenization. *Multiscale Modeling & Simulation*, 4(3):790–812, 2005.
- [39] Arif Masud and RA2203991 Khurram. A multiscale finite element method for the incompressible navier–stokes equations. *Computer Methods in Applied Mechanics and Engineering*, 195(13-16):1750–1777, 2006.
- [40] Thomas Y Hou and Xiao-Hui Wu. A multiscale finite element method for elliptic problems in composite materials and porous media. *Journal of computational physics*, 134(1):169–189, 1997.
- [41] Ibrahim Y Akkutlu, Yalchin Efendiev, and Maria Vasilyeva. Multiscale model reduction for shale gas transport in fractured media. *Computational Geosciences*, 20:953–973, 2016.
- [42] Eric T Chung, Yalchin Efendiev, Tat Leung, and Maria Vasilyeva. Coupling of multiscale and multi-continuum approaches. *GEM-International Journal on Geomathematics*, 8(1):9–41, 2017.

- [43] Yalchin Efendiev, Juan Galvis, and Thomas Y Hou. Generalized multiscale finite element methods (gmsfem). *Journal of Computational Physics*, 251:116–135, 2013.
- [44] Denis Spiridonov, Maria Vasilyeva, and Wing Tat Leung. A generalized multiscale finite element method (gmsfem) for perforated domain flows with robin boundary conditions. *Journal of Computational and Applied Mathematics*, 357:319–328, 2019.
- [45] Denis Spiridonov, Maria Vasilyeva, and Eric T Chung. Generalized multiscale finite element method for multicontinua unsaturated flow problems in fractured porous media. *Journal of Computational and Applied Mathematics*, 370:112594, 2020.
- [46] Patrick Jenny, Seong H Lee, and Hamdi A Tchelepi. Adaptive multiscale finite-volume method for multiphase flow and transport in porous media. *Multiscale Modeling & Simulation*, 3(1):50–64, 2005.
- [47] Irina Sokolova, Muhammad Gusti Bastisya, and Hadi Hajibeygi. Multiscale finite volume method for finite-volume-based simulation of poroelasticity. *Journal of Computational Physics*, 379:309–324, 2019.
- [48] Eric T Chung, Wing Tat Leung, and Maria Vasilyeva. Mixed gmsfem for second order elliptic problem in perforated domains. *Journal of Computational and Applied Mathematics*, 304:84–99, 2016.
- [49] Ferdinando Auricchio, L Beirão da Veiga, F Brezzi, and C Lovadina. Mixed finite element methods. *Encyclopedia of Computational Mechanics Second Edition*, pages 1–53, 2017.
- [50] Daniele Boffi, Franco Brezzi, Michel Fortin, et al. *Mixed finite element methods and applications*, volume 44. Springer, 2013.
- [51] Denis Spiridonov, Maria Vasilyeva, Min Wang, and Eric T Chung. Mixed generalized multiscale finite element method for flow problem in thin domains. *Journal of Computational and Applied Mathematics*, 416:114577, 2022.
- [52] Eric T Chung, Yalchin Efendiev, Wing Tat Leung, Maria Vasilyeva, and Yating Wang. Non-local multi-continua upscaling for flows in heterogeneous fractured media. *Journal of Computational Physics*, 372:22–34, 2018.
- [53] Maria Vasilyeva, Eric T Chung, Yalchin Efendiev, and Jihoon Kim. Constrained energy minimization based upscaling for coupled flow and mechanics. *Journal of Computational Physics*, 376:660–674, 2019.
- [54] Maria Vasilyeva, Eric T Chung, Siu Wun Cheung, Yating Wang, and Georgy Prokopev. Nonlocal multi-continua upscaling for multicontinua flow problems in fractured porous media. *Journal of Computational and Applied Mathematics*, 2019.
- [55] Eric T Chung, Yalchin Efendiev, and Wing Tat Leung. Constraint energy minimizing generalized multiscale finite element method. *Computer Methods in Applied Mechanics and Engineering*, 339:298–319, 2018.

- [56] Eric Chung, Yalchin Efendiev, and Wing Tat Leung. Constraint energy minimizing generalized multiscale finite element method in the mixed formulation. *Computational Geosciences*, 22:677–693, 2018.
- [57] Siu Wun Cheung, Eric T Chung, Yalchin Efendiev, Wing Tat Leung, and Maria Vasilyeva. Constraint energy minimizing generalized multiscale finite element method for dual continuum model. *Communications in Mathematical Sciences*, 18(3):663–685, 2020.
- [58] Eric T Chung, Yalchin Efendiev, and Wing Tat Leung. Residual-driven online generalized multiscale finite element methods. *Journal of Computational Physics*, 302:176–190, 2015.
- [59] Eric T Chung, Yalchin Efendiev, Wing Tat Leung, Maria Vasilyeva, and Yating Wang. Online adaptive local multiscale model reduction for heterogeneous problems in perforated domains. *Applicable Analysis*, 96(12):2002–2031, 2017.
- [60] Denis Spiridonov, Sergei Stepanov, et al. An online generalized multiscale finite element method for heat and mass transfer problem with artificial ground freezing. *Journal of Computational and Applied Mathematics*, 417:114561, 2023.
- [61] Denis Spiridonov, Maria Vasilyeva, Aleksei Tyrylgin, and Eric T Chung. An online generalized multiscale finite element method for unsaturated filtration problem in fractured media. *Mathematics*, 9(12):1382, 2021.
- [62] Denis Spiridonov, Jian Huang, Maria Vasilyeva, Yunqing Huang, and Eric T Chung. Mixed generalized multiscale finite element method for darcy-forchheimer model. *Mathematics*, 7(12):1212, 2019.
- [63] Maria Vasilyeva, Eric T Chung, Wing Tat Leung, Yating Wang, and Denis Spiridonov. Upscaling method for problems in perforated domains with non-homogeneous boundary conditions on perforations using non-local multi-continuum method (nlmc). *Journal of Computational and Applied Mathematics*, 357:215–227, 2019.
- [64] Lina Zhao and Eric T Chung. An analysis of the nlmc upscaling method for high contrast problems. *Journal of Computational and Applied Mathematics*, 367:112480, 2020.